# A Diagnostic Study of the Role of Remote Forcing in Tropical Atlantic Variability

A. CZAJA, P. VAN DER VAART, AND J. MARSHALL

*Department of Earth, Atmospheric, and Planetary Sciences, Massachusetts Institute of Technology, Cambridge, Massachusetts*

(Manuscript received 1 February 2002, in final form 5 June 2002)

ABSTRACT

This observational study focuses on remote forcing of the dominant pattern of north tropical Atlantic sea surface temperature (SST) anomalies by ENSO and NAO. Based on a spring SST index of the north tropical Atlantic (NTA) SST (5°–25°N), it is shown that almost all NTA–SST extreme events from 1950 to the present can be related to either ENSO or NAO. Since the SST NTA events lag NAO and ENSO events, NTA variability is interpreted as being largely a response to remote NAO or ENSO forcing.

The local response of the tropical Atlantic to these external sources—whether it be ENSO or the NAO—is observed to be rather similar: changes in surface winds induce changes in latent heating that, in turn, generate SST anomalies. Once generated, the latter are damped through local air–sea interaction, at a rate estimated to be 10 W $m^{-2}$ $K^{-1}$.

Experiments with simple models, but driven by observations, strongly suggests that variability on interannual to interdecadal timescales—both time series and spectral signatures—can be largely explained as a result of direct atmospheric forcing, without the need to invoke a significant role for local unstable air–sea interactions or ocean circulation.

## 1. Introduction

The dominant pattern of variability in sea surface temperature (SST) and surface winds over the tropical Atlantic is characterized by anomalous SST conditions north of the equator [the north tropical Atlantic (NTA)], cross-equatorial flow, and a modulation in the strength of the southeast and northeast trade winds (Nobre and Shukla 1996). As documented by various studies, these surface climate anomalies covary with changes in precipitation over the nordeste Brazil and subsaharan West Africa (see the recent review by Marshall et al. 2001).

Several mechanisms have been proposed to explain the origin of these interannual changes. One appealing scenario is that NTA variability might reflect coupled atmosphere–ocean interactions. This idea is motivated by the sensitivity of the atmosphere to tropical SST anomalies, and the potential for a large-scale positive feedback between changes in wind, evaporation, and SST (WES; Xie and Philander 1994). A warm NTA SST anomaly can induce a surface cross-equatorial flow with enhanced trades south of the equator and reduced trades north of the equator, in the form of a C-shaped anomalous circulation. The anomalous westerlies to the north of the equator may overlay the initial warm SST anomaly and enhance it through a reduction in surface evaporation because of lighter winds, thus providing a positive feedback. Idealized coupled models including ocean circulation and the WES feedback do indeed suggest that coupled dynamics might play a role in NTA variability on interannual to decadal timescales (Chang et al. 1997; Xie 1999), with the mean ocean circulation perhaps providing the damping (Chang et al. 2001; Seager et al. 2001).

Much of the NTA variability, however, could merely be a consequence of remote forcing by climate variability outside the tropical Atlantic. Strong candidates for such a remote forcing of NTA variability are ENSO (Covey and Hastenrath 1978; Curtis and Hastenrath 1995; Nobre and Shukla 1996; Enfield and Mayer 1997; Saravanan and Chang 2000) and the North Atlantic Oscillation (NAO; Grötzner et al. 1998; Czaja and Marshall 2001). ENSO and NAO events are indeed known to impact the trade winds over the Atlantic and the latter have been shown to be instrumental in driving NTA SST anomalies through their impact on latent heat exchange at the ocean surface (e.g., Halliwell and Mayer 1996; Carton et al. 1996). In this view, little role is required by ocean dynamics over the NTA region, as has been hinted at in several modeling studies (e.g., Carton et al. 1996; Halliwell 1998).

Giannini et al. (2001) view the competing influence of ENSO and the NAO on NTA variability as a modulation of ENSO teleconnections to the tropical North Atlantic. But more fundamentally, might NTA SST variability simply reflect the Atlantic signature of the

*Corresponding author address:* Dr. A. Czaja, Department of Earth, Ocean and Planetary Sciences, Massachusetts Institute of Technology, Rm. 54-1421, 77 Massachusetts Avenue, Cambridge, MA 02139.
E-mail: czaja@ocean.mit.edu

© 2002 American Meteorological Society

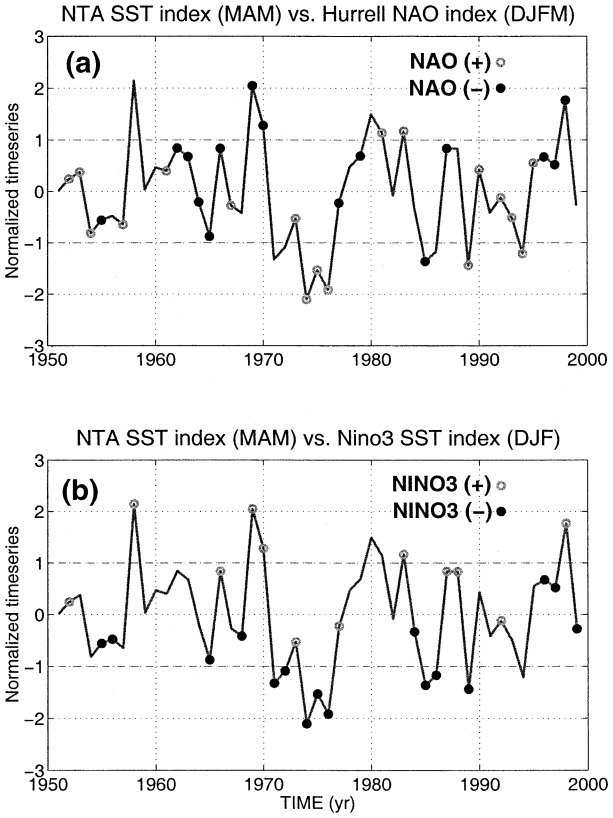


FIG. 1. Normalized NTA SST index time series from NCEP–NCAR (continuous curve) with years of high (larger than 0.5 std dev) and low (lower than −0.5 std dev) phases of (a) NAO and (b) ENSO, indicated as gray and black circles, respectively. The year refers to the Jan month in the definition of the NAO and Niño-3 indices.

warming–cooling of the tropical belt associated with ENSO, and the tropical Atlantic signature of the NAO-forced SST tripole in the North Atlantic (the so-called ''southern lobe'' of the tripole)? In this paper we address this question quantitatively and base our analysis on an SST index defined over the NTA region (5°–25°N, 60°–20°W) and averaged over time from March–April–May (MAM). This particular index is chosen because it captures the center of action of the dominant mode of NTA SST variability (e.g., Nobre and Shukla 1996; Dommenget and Latif 2000) that is most pronounced in spring (Nobre and Shukla 1996). Unless explicitly mentioned, all data considered are from the National Centers for Environmental Prediction–National Center for Atmospheric Research (NCEP–NCAR) reanalysis over the period 1950–99 (Kalnay et al. 1996; Trenberth et al. 2001).

The paper is structured as follows. First we show that almost all major NTA SST events observed over 1950–99 can be related to NAO or ENSO anomalies (section 2). We then investigate the mechanism behind this influence (section 3), and derive a simple model to simulate NTA variability (section 4). A discussion of the frequency dependence of ENSO and NAO forcing is given in section 5. Conclusions are offered in section 6.

TABLE 1. Statistics based on Fig. 1. The number of positive and negative (in parentheses) NAO and ENSO events are given, as well as the number of total high and low NTA events (amplitude larger than one std dev). The months over which the indices are defined are given in parentheses.

| NTA index (MAM) | NAO (DJFM) | ENSO (DJF) | Neither NAO nor ENSO | Total |
|---|---|---|---|---|
| ≥+1 std dev | 2 (3) | 5 (0) | 1 | 7 |
| ≤−1 std dev | 5 (1) | 0 (8) | 0 | 9 |

## 2. A simple partitioning of NTA variability

As a simple way to study the dependence of NTA variability on NAO and ENSO, we show in Fig. 1 the NTA SST index (continuous curve in Figs. 1a,b) along with years of high and low phases of the NAO (Fig. 1a) and ENSO (Fig. 1b), as indicated by gray and black circles, respectively. The NAO and ENSO phases are determined from the wintertime (DJFM) sea level pressure (SLP) index of Hurrell (1995) and the so-called Niño-3 (5°S–5°N, 90°–150°W) SST index (Philander 1990) in winter (DJF), respectively (all climate indices used in this study were downloaded from the NCAR Climate Analysis Section Data Catalog available online at http://goldhill.cgd.ucar.edu/cas/catalog/). Consistent with the idea that NAO and ENSO are independent modes of climate variability, the correlation between the two indices is not significant (0.05). Note that all time series considered in this study have been linearly detrended prior to any computation or display.

The visual impression from Fig. 1a is that negative NAO events tend to be associated with warm NTA conditions, and positive NAO events with cold NTA conditions. More often than not [about two-thirds of the low (high) NAO events correspond to warm (cold) NTA conditions] strong NAO events are clearly identifiable in the NTA SST index time series (e.g., the low NAO phase of 1969 or the high NAO phase of 1989). An opposite phase relationship is found between the NTA and ENSO indices (Fig. 1b). One sees that warm El Niño years are typically associated with warm NTA conditions (three-fourths of the positive Niño-3 events), the reverse situation being seen even more frequently during La Niña years (seven-eighths of the negative Niño-3 events are associated with cold NTA conditions). On occasions, NAO and ENSO add constructively to create NTA anomalies (e.g., the coldest NTA conditions seen in Fig. 1 during the mid 1970s), but they also tend to cancel one another at other times (e.g., the impact of the strong ENSO event of 1983 is reduced owing to positive NAO conditions that year). Similar conclusions were reached by Giannini et al. (2001) based on a linear regression analysis over 1949–99.

Table 1 summarizes the analysis of the NTA index.

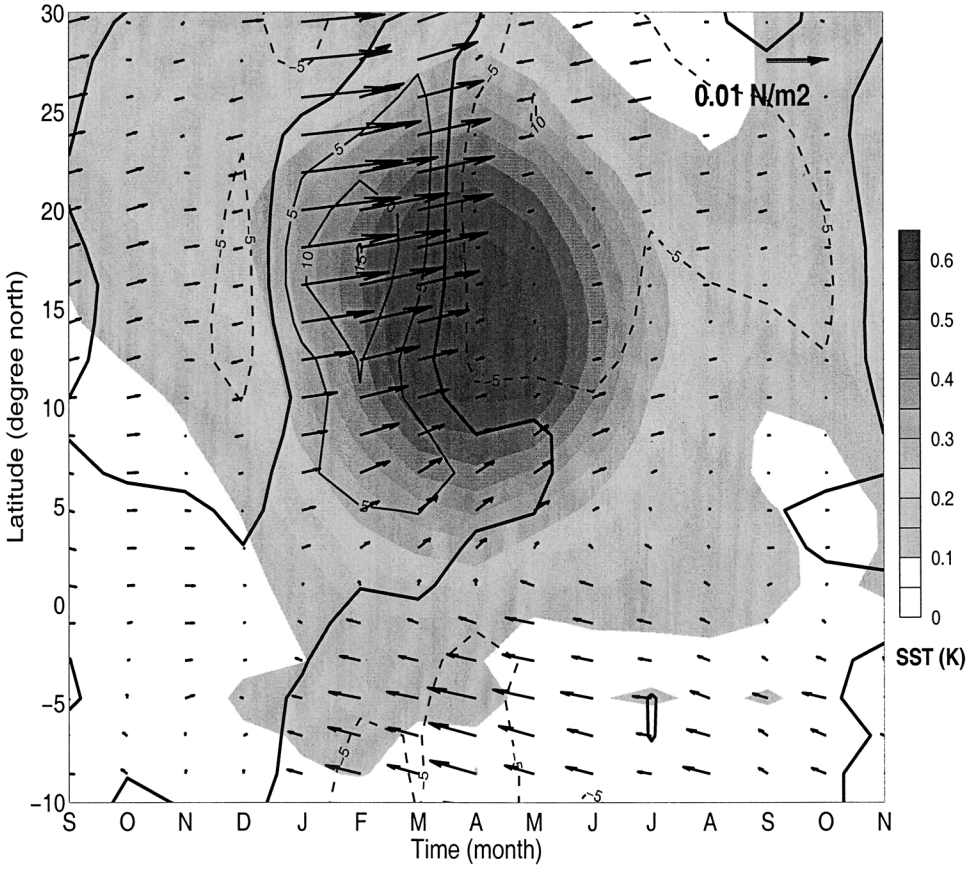


FIG. 2. Regression map of surface wind stress (arrows, scale in the top-right corner); net surface heat flux (contoured every 5 W $m^{-2}$, positive into the ocean, dashed when negative, zero contour thickened); and SST (shaded, in K) onto the NTA SST index time series in MAM.

Over seven strong warm NTA events, only one (in 1980) was not either related to ENSO or the NAO. All nine strong cold NTA events are either related to ENSO or the NAO. We emphasize that the NAO and ENSO indices used are defined in winter (DJFM and DJF, respectively), whereas the NTA index is defined the following spring (MAM). The previous associations are thus suggestive of a significant predictive skill of NTA variability solely based on preceding NAO or ENSO events. We examine below the physical mechanisms that are responsible for these lagged associations.

## 3. Mechanisms governing NTA variability

### *a. The development and decay of an anomalous NTA event*

To document the relationship between anomalies in surface wind stress, net surface heat flux, and SST during the development and decay of anomalous NTA events, we have regressed these fields onto the NTA SST index (Fig. 2). The regression map shows the surface wind (arrows), net surface heat flux (contours), and SST (shading) anomalies are associated with a one standard deviation change in the NTA SST index. It is displayed as a function of latitude (10°S–30°N, *y* axis) and time lag (from the fall prior to the warm spring NTA event to the following fall, *x* axis). All fields were averaged zonally between 40° and 20°W. The regression map for SST shows a warm anomaly centered in spring (MAM) between 10° and 20°N, consistent with the definition of the NTA index (SST averaged over 5°–25°N and MAM—see introduction). The anomalous SST pattern persists through the following fall, indicating a typical persistence time of about 6 months.

The map for the surface wind is dominated by winter (JFM) anomalous westerly winds centered along 20°N, with a typical meridional scale of 10°. The westerly wind anomalies reflect a weakening of the trades prior (1–2 months) to the warm NTA event, and are likely to be primarily responsible for the generation of the event through reduced evaporative loss over the NTA region (see Figs. 3b,c). North of 10°N, the wind anomaly persists from January to March and subsequently disappears, which we interpret as reflecting the persistence of NAO and ENSO, and a negligible feedback of NTA SST onto the 10°–30°N wind anomalies (see sections

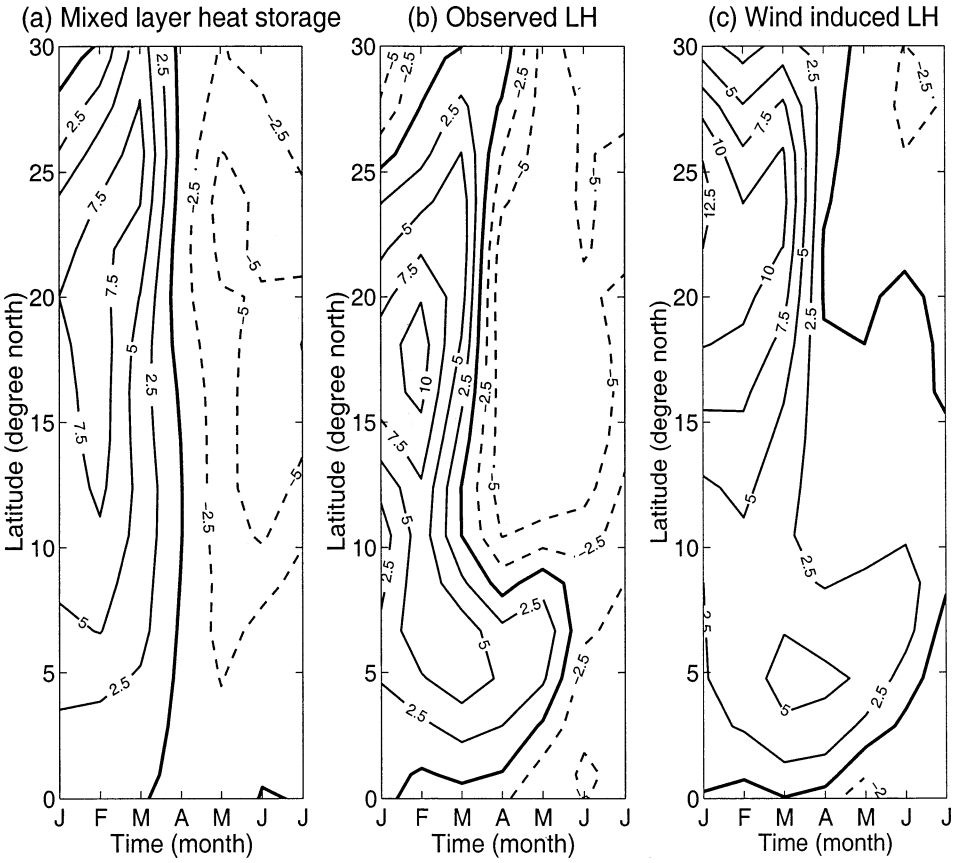


FIG. 3. Same as Fig. 2 but for (a) mixed layer heat storage, (b) latent heating, and (c) wind-induced changes in latent heating. All fields are in W $m^{-2}$ with a contour interval of 2.5 W $m^{-2}$. The SST tendency was computed from Fig. 2 using the finite difference in time.

3a and 4). South of 10°N, however, we observe a simultaneous evolution of anomalous SST and northward winds across the equator from January to July, with a strengthening of the southeast trades south of the equator and a weakening of the northeast trades north of the equator in the form of a C-shaped anomalous circulation. The latter reflects a northward shift of the spring intertropical convergence zone (ITCZ). Since various observational (Hastenrath and Greischar 1993; Chiang et al. 2002), and modeling studies suggest a similar and robust anomalous circulation forced by warm NTA SST anomalies (Chang et al. 2000; Sutton et al. 2000; Chiang et al. 2001), it seems likely that the ITCZ shifts northward in response to the warm SST anomaly peaking in MAM. According to this interpretation, the persistence of wind anomaly south of 10°N would then reflect the persistence of the NTA SST anomaly itself.

The pattern of anomalous net surface heat flux (contoured in Fig. 2, positive into the ocean as continuous curve) indicates anomalous warming of the ocean prior to the warm spring SST anomaly (continuous contours in JFM over 5°–25°N) and anomalous cooling north of 10°N afterward (dashed contours), but note that the surface warming persists through spring in the deep Tropics (see below). Further analysis indicates that the net heating–cooling anomalies are almost entirely due to latent heating anomalies. To check quantitatively that the latter are responsible for the generation and decay of the warm SST anomaly, we compare the mixed layer heat storage $\rho C_p \bar{h} dT/dt$ (Fig. 3a; where $\rho$ is the density of seawater, $C_p$ its heat capacity, and $\bar{h}$ the seasonally and latitudinally varying mixed layer depth from Levitus and Boyer 1994) with the observed changes in latent heating (Fig. 3b). Over the core of the NTA SST anomaly (10°–20°N) there is a good agreement between both fields before and after spring, indicating that latent heating is not only generating the SST anomaly but is also damping the SST anomaly once it is generated. The damping heat flux is about 5 W $m^{-2}$ for a 0.5-K SST anomaly (Fig. 2), implying a damping rate of about 10 W $m^{-2}$ $K^{-1}$. This damping rate is in agreement with that estimated by Frankignoul and Kestenare (2001, manuscript submitted to *Climate Dyn.*). Since wind anomalies over the core of the NTA SST anomaly (10°–20°N) disappear by the time the latter has reached its peak (Fig. 2), the damping strength of 10 W $m^{-2}$ $K^{-1}$ should only be set by mean wind speed and the local adjustment of temperature and moisture in the atmospheric boundary layer

to the NTA SST anomaly (Frankignoul et al. 1998). Note that for a typical mixed layer depth of 40 m, 10 W $m^{-2}$ $K^{-1}$ amounts to a persistence time of 6 months, consistent with that suggested in Fig. 2.

Figure 3b indicates a slightly larger heating rate than accounted for by mixed layer storage (Fig. 3a) in winter (JFM) north of 10°N. This is consistent with the impact of anomalous Ekman currents on SST, which is expected to oppose the latent heating anomaly (reduced trades leading to reduced northward heat transport over the NTA region and anomalous cooling of SST). The small difference hinted at in Figs. 3a,b amounts to a couple of W $m^{-2}$, less than 20% of the evaporative forcing.

The observed changes in latent heating over the deep Tropics in spring (Figs. 2, 3b) imply a sustained warming of the SST anomaly rather than a damping, as found north of 10°N. To elucidate the origin of this warming we have computed the changes in latent heating induced by changes in wind speed using bulk formulas (Fig. 3c; see the appendix for details of the computation) and have compared them to the observed changes in latent heating (Fig. 3b). It is found that the heating south of 10°N in spring is explained by the changes in the surface winds during that time, that is, by the cross-equatorial flow and its related weakening of the northeast trades. To the extent that these wind changes are indeed a response to the warm SST anomaly, as suggested above, Fig. 3c is indicative of a positive feedback (the WES mechanism, see introduction) in spring, extending from the equator to about 15°N. Note, however, that it is only in the deep Tropics (south of 10°N) that the WES feedback dominates over the local damping, since Fig. 3b indicates a net cooling of the warm SST anomaly north of 10°N. Both the increase of the local damping with mean wind speed (see Frankignoul et al. 1998) and the stronger wind-induced latent heating near 5°N (Fig. 3c) contribute to the confinement of the WES feedback to the deep Tropics. It has not been attempted to diagnose further which processes balance the (WES-related) latent heating in the deep Tropics (possibly mean advection by the ocean, as suggested by Chang et al. 2001; Seager et al. 2001) since the core of the NTA SST anomaly (the focus of this study) is found northward of 10°N, and is overall not affected by the WES mechanism.

Finally, note that no indication was found that the SST anomaly regressed onto the NTA SST index could become negative south of the equator when extending Fig. 2 to 30°S (not shown). Thus, our analysis does not support the ''dipole SST mode'' invoked by various authors (e.g., Chang et al. 1997; Xie 1999).

### b. Impact of ENSO and NAO on anomalous NTA events

The previous section suggests the following scenario. A warm spring NTA event is initiated by a reduction in surface evaporative loss (associated with reduced trades) over the NTA region in winter. The latter is explained mostly by a reduction in the strength of the trade winds, as suggested by this study (Figs. 2, 3c) and others (e.g., Halliwell and Mayer 1996). Once the SST anomaly is created (late winter to spring) it releases its heat content to the atmosphere locally through enhanced evaporation at a rate estimated to be $\simeq$10 W $m^{-2}$ $K^{-1}$. Since the analysis in section 3a is linear, the reverse chain of arguments apply to cold NTA events. The strong impact of ENSO and NAO onto NTA demonstrated in section 2 should thus simply result from a modulation of the strength of the trade winds in winter.

Figure 4 is a correlation map of the wintertime sea level pressure (SLP) anomaly onto the Niño-3 (Fig. 4a) and Hurrell's NAO (Fig. 4b) indices. One recovers the north–south dipole characteristic of the NAO, with a positive NAO event associated with a stronger subtropical high. The map for Niño-3 shows more of a southwest to northeast orientation, with an opposite pressure anomaly over the western subtropical gyre and the tropical Atlantic basin. It has been suggested that the negative pressure anomaly over the western subtropical gyre is part of the Pacific–North American (PNA) pattern forced by positive ENSO events, while the positive pressure anomaly found in the Tropics reflects a shift of the Walker circulation (Klein et al. 1999). From Fig. 4, ENSO and NAO anomalies in SLP are thus indeed expected to modulate the strength of the trade winds over the NTA region, but with positive NAO and ENSO events opposing each other, as was found in section 2. Table 2 further illustrates this point by comparing the NAO and ENSO indices to an index of the trade winds (zonal surface wind stress anomalies averaged over 10°–30°N, 40°–20°W in JFM), as was done for the NTA SST index in Table 1. Again, a clear separation of strong anomalous trade events as a function of NAO and ENSO is indicated, with only 2 out of 17 events not explained by either NAO or ENSO.

A regression analysis similar to that of Fig. 2 is shown in Fig. 5 but based on ENSO and NAO indices. Positive ENSO events are associated with anomalous westerlies (Fig. 5a) inducing heating over the NTA region at a rate of about 10 W $m^{-2}$. Once the surface wind anomaly disappears in spring, the surface heat flux changes sign over the SST anomaly and damps the latter, except again between 5° and 10°N in spring. Consistent with section 3 and with Klein et al.'s (1999) results, the regression map for the net surface heat flux is largely dominated by changes in latent heating with little contribution from radiative and sensible flux (not shown). The regression map based on the *negative* NAO index (Fig. 5b) shows basically the same pattern of surface heating–cooling of SST over 10°–20°N (the core of the NTA SST event), although the map differs somewhat from that based on Niño-3 south of 5°N. Note also the different persistence of 10°–30°N wind anomalies for ENSO (JFM) and NAO (JF) regression maps. This is likely to have resulted from the persistence of ENSO and NAO themselves, with no

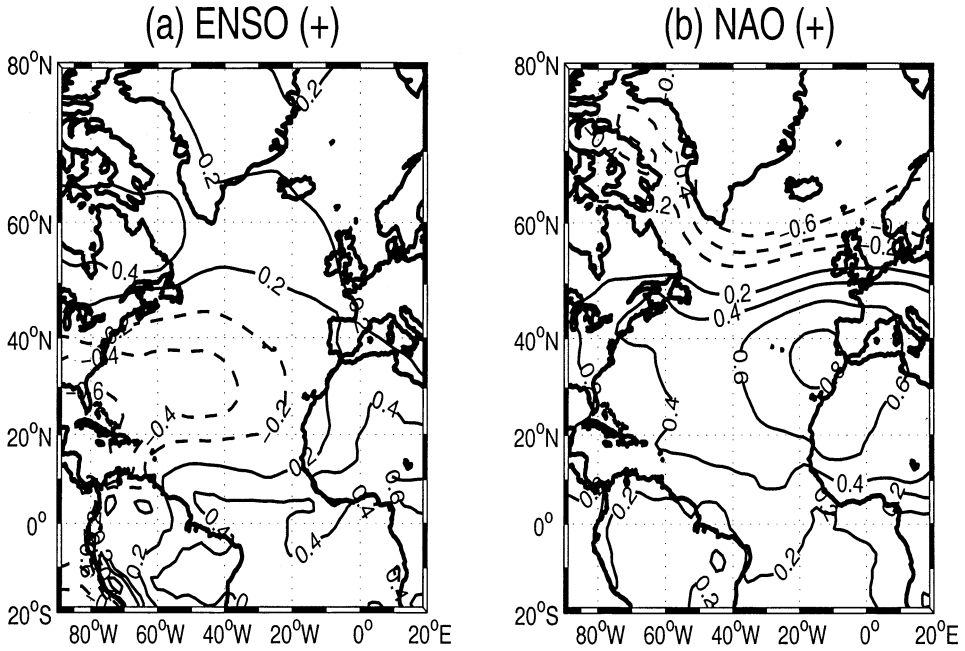


FIG. 4. Correlation map of wintertime (JFM) SLP anomaly and (a) DJF Niño-3 SST index, and (b) DJFM NAO index of Hurrell. Correlations are contoured every 0.2, dashed when negative. The zero contour is omitted. A correlation of 0.3 is significant at the 95% level, assuming independent samples. The NAO and ENSO indices are the same as those used in Fig. 1.

additional memory added to the wind anomaly by the local interaction with the NTA SST. This latter point—negligible feedback of NTA SST anomaly on the 10°–30°N surface wind—is further discussed in section 4.

In summary, a similar mechanism is responsible for the forcing of NTA variability by both ENSO and NAO. It consists in a modulation of latent heating through changes in trade wind speeds and a subsequent local damping through air–sea interactions. The fact that almost all strong NTA SST and trade winds events can be related to either NAO or ENSO (Tables 1 and 2) suggests that a simple model driven by observed NAO and ENSO wind anomalies should capture NTA variability. This is studied in the next section.

## 4. A simple model for NTA variability

Let us assume, motivated by the previous section, that SST anomalies over the NTA region are essentially driven by changes in latent heating. That is,

$$\rho C_p h_0 \frac{dT}{dt} = F_{\text{lat}}, \tag{1}$$

where $h_0$ is an annual mean mixed layer depth ($h_0 =$ 40 m is found when averaging $\overline{h}$ over time and latitude), $F_{\text{lat}}$ the latent heating (positive when warming the ocean), and $T$ the SST, all fields averaged over the NTA region (5°–25°N, 60°–20°W).

As a simple index of wind anomalies associated with NAO and ENSO, Fig. 4 suggests that we average SLP anomalies north of the NTA region, say 20°–40°N, 70°–10°W.[1] Positive anomalies of that index (denoted by STH for subtropical high) reflect a strengthening of the trades and yield enhanced evaporative loss over the NTA region ($F_{\text{lat}} < 0$). Since anomalous heating is also affected by the SST anomaly, once the latter is generated, we write

$$F_{\text{lat}} = -\alpha\ \text{STH} - \gamma T, \tag{2}$$

where $\alpha$ (positive, in W m$^{-2}$ mb$^{-1}$) scales a change in the strength of the subtropical high into a change in latent heating, and $\gamma$ (in W m$^{-2}$ K$^{-1}$) measures the sensitivity of $F_{\text{lat}}$ to SST. Combining (1) and (2), we obtain

$$\rho C_p h_0 \frac{dT}{dt} = -\alpha\text{STH} - \gamma T. \tag{3}$$

TABLE 2. Same as Table 1 but for an index of the trade winds (see text for a definition). A positive value of the trade wind index indicates anomalous westerly wind, i.e., reduced trade winds.

| Trade winds index (JFM) | NAO (DJFM) | ENSO (DJF) | Neither NAO nor ENSO | Total |
|---|---|---|---|---|
| ≥+1 std dev | 0 (7) | 6 (1) | 1 | 9 |
| ≤−1 std dev | 5 (0) | 0 (4) | 1 | 8 |

[1] The choice of an SLP index rather than wind stress will allow us to use the long record of reconstructed SLP anomalies of Kaplan et al. 2000 (see below).

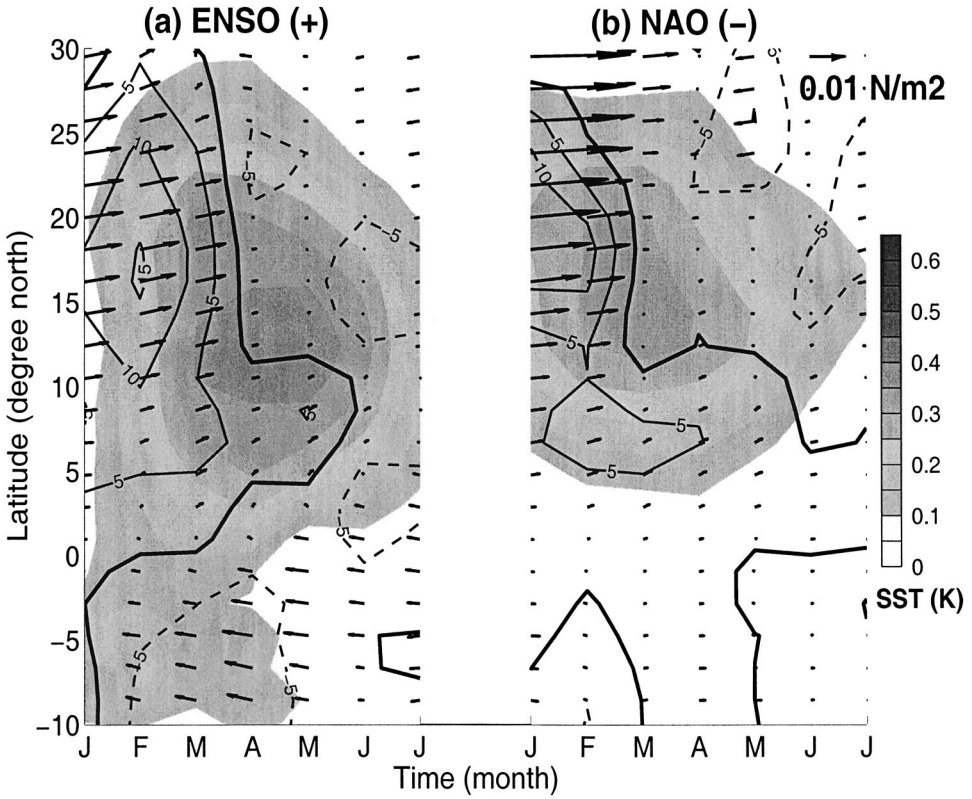


FIG. 5. Same as Fig. 2 but regressed onto (a) Niño-3 SST index, and (b) *negative* NAO index.

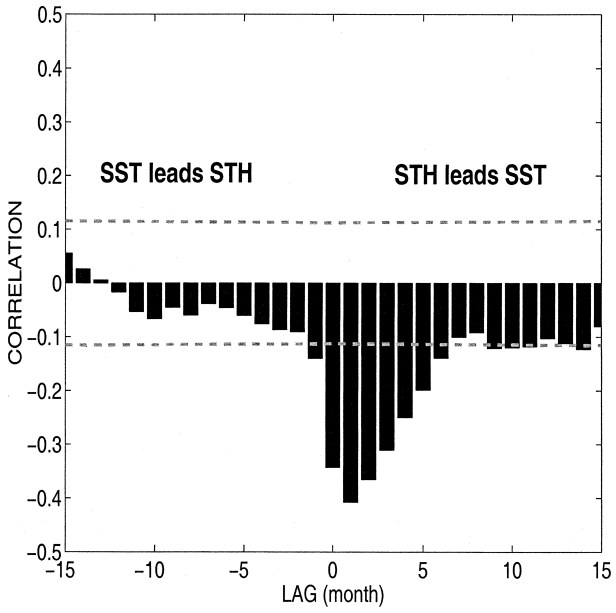


FIG. 6. Cross-correlation function between the monthly NTA SST and STH indices (see text for a definition). STH leads at positive lags (in months). The dashed gray lines indicate an approximate 95% confidence level, taking into account the month-to-month persistence of the STH index.

The latter model is probably the simplest proposed so far for NTA variability. It is close to that of Frankignoul and Hasselman (1977) for extratropical SST anomalies. Note, however, that the forcing (the STH index) is slightly red, rather than white as in Frankignoul and Hasselman (1977), because of the influence of NAO and ENSO on the subtropical high. It is assumed that the strength of the subtropical high is not affected by the NTA SST anomaly, so that the only feedback included in the model is the local damping effect of latent heating. This assumption is supported by an analysis of the correlation between NTA SST and STH (Fig. 6). The correlation function is strongly asymmetric with temporal lag, having a minimum when SST lags by one month (strong STH drives cold SST), and not being significant when SST leads STH. This is a known signature of one-way forcing of the ocean by the atmosphere (e.g., Frankignoul 1985).[2] Note that very similar results are obtained when the trade wind index of Table 2 rather than STH is used when computing the cross-correlation function (not shown).

The model (3) has two parameters, $\alpha$ and $\gamma$. As detailed in the appendix, the scaling factor $\alpha$ can be rough-

[2] Note that the marginal correlation observed in Fig. 6 when SST leads STH by one month is likely to reflect the month-to-month persistence of the subtropical high, rather than a feedback of the NTA SST anomaly onto the subtropical high (e.g., Frankignoul et al. 1998).

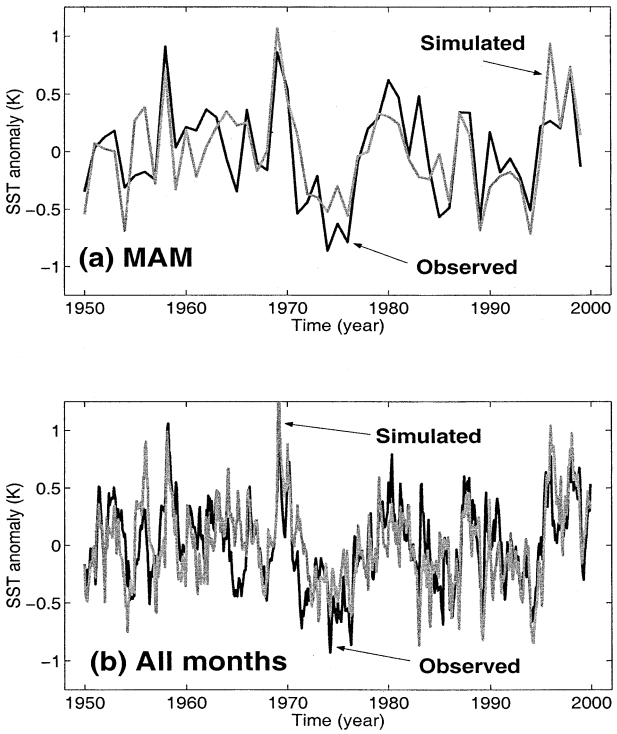


FIG. 7. Observed (black) and simulated (gray) NTA SST indices (in K) over the period 1950–99: (a) spring (MAM averaged) anomalies, and (b) all months.

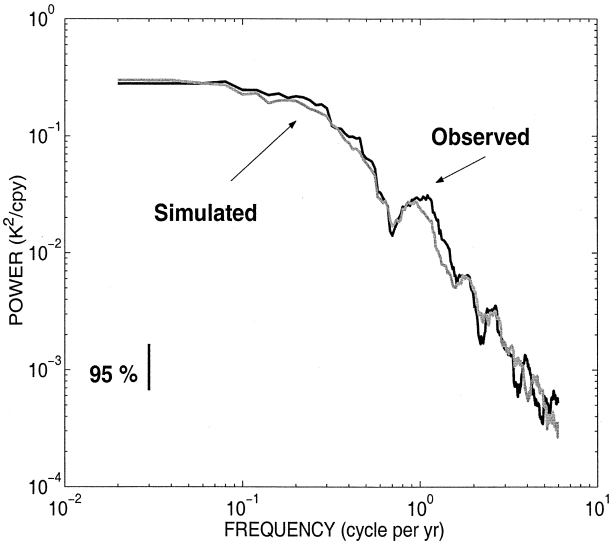


FIG. 8. Power spectrum of observed (black) and simulated (gray) NTA SST indices from Fig. 7b. The frequency is expressed in cycles per year (cpy) and the power spectrum in $K^2$ $cpy^{-1}$. The spectrum was estimated using the multitaper method (Percival and Walden 1993), after linearly detrending the time series. The vertical line gives the 95% confidence level on the spectral estimate.

ly estimated from bulk formulas and regression analysis of surface wind onto the STH index, yielding a value $\alpha \simeq 6$ W m$^{-2}$ mb$^{-1}$. Note that a strengthening of the subtropical high rapidly (on an inertial period) sets a stronger northward Ekman heat transport over the NTA region, which reduces the evaporative forcing of the NTA SST anomaly, and can also be modeled by an $\alpha$ term in (3). This opposing effect was estimated to be less than 20% in section 3a, which is probably in the error bar of our estimate of $\alpha$. Accordingly, we keep $\alpha = 6$ W m$^{-2}$ mb$^{-1}$ for simplicity. The sensitivity $\gamma$ was estimated to be $\gamma \simeq 10$ W m$^{-2}$ K$^{-1}$ in section 3a. Using these values one can integrate (3) forward in time and simulate the time history of the NTA SST index from the knowledge of the monthly time series of the subtropical high index.

The resulting hindcast NTA SST time series is compared to the observed time series in Fig. 7 (Fig. 7a for the spring season, Fig. 7b for all months). One observes that most of the strong positive and negative events are well reproduced (e.g., positive events of 1958, 1969, and 1998; negative events of the mid-1970s, 1989, and 1994), as are the decadal fluctuations (low conditions of the 1970s and the 1990s, and the subsequent upward trend). The temporal correlation between the simulated and observed monthly NTA index is high (0.7), and it even slightly increases when only the spring period is considered (0.72). Analysis in the frequency domain shows significant coherence between observed and simulated time series on a broad range of timescales, with about 60% of the variance captured at decadal timescales (not shown). The spectra of the simulated and observed time series are almost indistinguishable (Fig. 8).

## 5. Frequency dependence of remote ENSO and NAO forcing

The previous analysis, although strongly suggestive of NTA variability being driven by NAO and ENSO, does not quantitatively assess the relative importance of ENSO and NAO and the frequency dependence of their impact on NTA variability. The short record (50 yr) studied here clearly limits our ability to partition the variance into frequency bands, and so we consider a longer record of NTA SST, ENSO, and NAO indices. These were obtained from the Kaplan et al. (1997) SST dataset averaged over the NTA region in MAM, an updated Darwin SLP record in DJF (Trenberth 1984), and the previously used NAO index of Hurrell in DJFM (1995), respectively. The overlapping period covered by these indices is 1882–1992 (110 yr).

Figure 9 shows the squared coherence (Fig. 9a) and phase (Fig. 9b) between the NTA SST index and ENSO (gray) and the NTA SST index and NAO (black). Interestingly, the cospectral analysis reveals a simple partitioning: ENSO dominates over NAO at interannual timescales (2–7 yr) but NAO dominates over ENSO on timescales longer than decadal. In these respective frequency bands the phase is stable (Fig. 9b), with an in-phase relationship between ENSO and NTA SST (warm

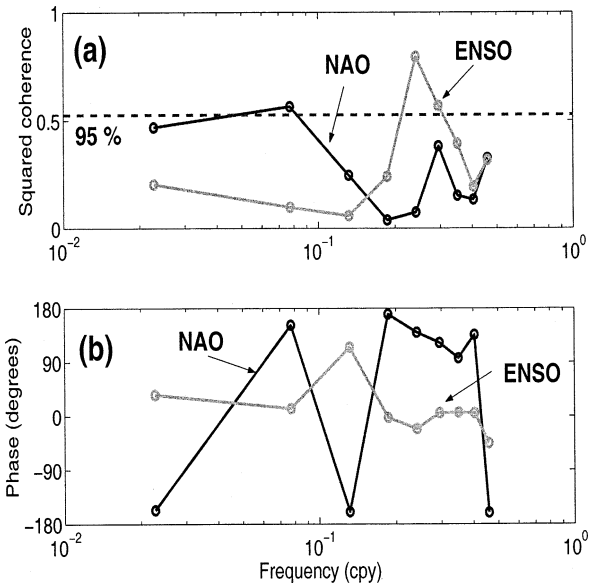


FIG. 9. Cospectral analysis of NTA SST and ENSO (gray), and NTA SST and NAO (black) indices. (a) Squared coherence (the horizontal dashed line gives an approximate 95% confidence level), and (b) phase (in degrees). The cospectra were estimated using a Daniell window (averaged over six frequency bins).

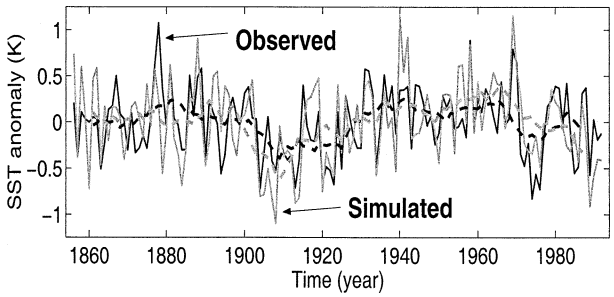


FIG. 10. Time series of simulated (gray) and observed (black) NTA SST in MAM (in K). Dashed lines indicate 10-yr running mean.

ENSO events covary with warm NTA SST events) but out-of-phase relationship ($\pm 180°$) between NAO and NTA SST (positive NAO events covary with cold NTA SST events), in agreement with previous sections. From Fig. 9a, typically 70% of the NTA SST variance at interannual timescales can be attributed to ENSO. NAO is seen to account for 50% of the low-frequency (decadal and interdecadal timescales) fluctuations of the NTA SST index.

If the stronger coherence found with ENSO at timescales of 2–7 years can be expected from the broadband peak displayed by the Niño-3 index in that band, the frequency dependence of the coherence between NTA SST and NAO is more intriguing because Hurrell's NAO index is only weakly red (Wunsch 1999). An interesting possibility could be that the dominance of NAO over ENSO at long timescales might result from changes in the North Atlantic meridional overturning circulation (MOC) in addition to the evaporative forcing encapsulated in (1). Indeed, both NAO and MOC have been suggested to covary at interdecadal timescales, with large related changes in ocean heat transport at 25°N (e.g., Häkkinen 1999; Eden and Jung 2001), which could impact NTA SST variability. To clarify the relevance of the model (3) at these long timescales we have integrated (3) forward in time using a long time series of the STH index from Kaplan et al.'s (2000) SLP data (1856–1992), and the same $\alpha$ and $\gamma$ as in section 4. In the resulting spring (MAM), the NTA SST index is compared to that from the Kaplan et al.'s (1997) SST data in Fig. 10, with a 10-yr running mean indicated as dashed lines. Again, one observes a good agreement between simulated (gray) and observed (black) time series at interannual timescales (the correlation of the raw time series is 0.62). However, even better agreement is found for the low-pass time series (the negative SST tendency of 1880–1910, the positive tendency of 1920–60, and the subsequent negative tendency). Overall, Fig. 10 strongly suggests that the model (3) is relevant at decadal and longer timescales, and that geostrophic ocean dynamics is of secondary importance even at these long timescales in the hindcast of NTA SST variability. The weakness of mean SST gradients over 5°–25°N might limit the impact of changes in ocean circulation on the oceanic mixed layer heat budget at these latitudes, and possibly explain the good simulation of the interdecadal changes in Fig. 10, but a complete explanation requires further modeling studies. We note that, on the long term, ocean heat transport divergence–convergence is also not crucial over the NTA region, since net radiation and evaporation approximately balance each other when annually and meridionally averaged over the latitude band 5°–25°N (not shown).

## 6. Conclusions

Almost all strong anomalies in the north tropical Atlantic (NTA) SST observed from 1950 to the present can be accounted for by prior ENSO or NAO events. The NAO and ENSO influence is felt through the semipermanent subtropical high pressure system and the related trade winds, whose intensity modulates the latent heating at the ocean surface. Once generated, a warm NTA SST anomaly releases its energy to the atmosphere through enhanced evaporation at a rate of $\simeq 10$ W m$^{-2}$ K$^{-1}$. This local process sets the persistence of the anomaly (about 6 months); the positive (WES) feedback hinted at in our study occurs too far to the south (0°–10°N) to significantly impact the evolution of the NTA SST anomaly. A simple model combining these elements, Eq. (3), is successful in simulating NTA variability on timescales ranging from interannual to interdecadal.

On the evidence of the observations and models analyzed here, there does not appear to be significant intrinsic north tropical Atlantic variability. Local geostrophic ocean dynamics and large-scale unstable air–

sea interactions do not have to be invoked to explain low-frequency fluctuations in this region. The fluctuations in NTA SST seem to arise largely as a mirror image of the changes in the strength of the subtropical high, with little indication that they can feed back significantly upon the latter. The results presented here contrast with those obtained with the mid- to high-latitude SST anomaly of the North Atlantic. There, the pronounced departure from red noise–type spectra observed in the long record of SST (e.g., Czaja and Marshall 2001) suggests a stronger role for ocean circulation than in the north tropical Atlantic.

*Acknowledgments.* The authors were supported by a grant from the National Oceanic and Atmospheric Administration.

## APPENDIX

### Surface Latent Heating Sensitivity to Wind Changes

Denoting the density of air by $\rho_a$, its specific humidity by $q_a$, the saturation specific humidity at the sea surface temperature by $q_s$, and the wind speed by $w$, the evaporation flux $E$ over the ocean can be written (Gill 1982) as

$$E = \rho_a C_E w(q_s - q_a), \tag{A1}$$

where $C_E$ is a dimensionless coefficient. The latent heating is $F_{\text{lat}} = L_v E$, where $L_v = 2.5 \times 10^6$ J kg$^{-1}$ is the latent heat of vaporization of water.

Decomposing the wind speed as $w = \sqrt{u^2 + v^2 + w_*^2}$ where $(u, v)$ are the zonal and meridional wind velocities 10 m above the ocean, and $w_*$ is a turbulent background wind speed (Xie and Philander 1994), a change $\delta u$ in zonal wind induces a change $\delta F_{\text{lat}}$

$$\delta F_{\text{lat}} = L_v \rho_a C_E (q_s - q_a) \frac{u}{w} \delta u, \tag{A2}$$

where variables other than $u$ have been kept constant. For small $\delta u$ we approximate the ratio of changes to a derivative so that

$$\frac{\partial F_{\text{lat}}}{\partial u} = L_v \rho_a C_E (q_s - q_a) \frac{u}{w} \tag{A3}$$

and likewise for a change in meridional wind

$$\frac{\partial F_{\text{lat}}}{\partial v} = L_v \rho_a C_E (q_s - q_a) \frac{v}{w}. \tag{A4}$$

A change $(\delta u, \delta v)$ in wind vector thus induces a change in latent heating

$$\delta F_{\text{lat}} = \frac{\partial F_{\text{lat}}}{\partial u} \delta u + \frac{\partial F_{\text{lat}}}{\partial u} \delta v = L_v \rho_a C_E (q_s - q_a) \frac{u \delta u + v \delta v}{w}. \tag{A5}$$

In this study, we have approximated the zonal average of $\delta F_{\text{lat}}$ in (A5) by the $\delta F_{\text{lat}}$ change obtained with zonally averaged $u$, $v$, $w$, $q_s$, $q_a$, $\delta u$, and $\delta v$ in (A5). This is justified by the fact that over the zonal belt considered (at most 60°–20°W) the variables in (A5) do not vary much with longitude. Note also that all variables are seasonally varying (except $w_*$ and $C_E$, which are constant in space and time—see below), so that the change $\delta F_{\text{lat}}$ can be computed for each month. The required mean seasonal cycle of $u$, $v$, $w$, $q_s$, and $q_a$ was constructed from the NCEP–NCAR reanalysis over the period of study 1959–99, while the $(\delta u, \delta v)$ were estimated by regression onto a specified climate index (NTA SST for Fig. 3c, STH–SLP for $\alpha$).

TABLE A1. Annual and latitudinal averaged $\delta F_{\text{lat}}$ (in W m$^{-2}$) induced by a one std dev change in the STH–SLP index described in the main text. The result is given for various background turbulent velocities $w_\star$ (over the range 0.5–4 m s$^{-1}$) and constant $C_E$ (expressed as fraction of $C_E^{\text{ref}}$ where $C_E^{\text{ref}} = 1.5 \times 10^{-3}$ is a reference value given in Gill 1982).

| $(\frac{C_E}{C_E^{\text{ref}}}/w_\star)$ | Turbulent velocity $w_\star$ | | | |
|---|---|---|---|---|
| | 0.5 | 1 | 2 | 4 |
| 0.5 | 5 | 4.9 | 4.5 | 3.8 |
| 1 | 10 | 9.8 | 9.1 | 7.5 |
| 2 | 20 | 19.5 | 18.2 | 15 |

The technique is clearly sensitive to the choice of the constants $w_*$ and $C_E$. Table A1 illustrates the change $\delta F_{\text{lat}}$ induced by a one standard deviation change in the STH–SLP index for plausible choices of $w_*$ and $C_E$ (note that in Table A1, $\delta F_{\text{lat}}$ was furthermore averaged over the annual cycle and the latitude band 5°–25°N). The sensitivity to $C_E$ is linear, as expected from (A5), and overall dominates that associated with $w_*$. The parameter $\alpha$ was deduced by averaging the numbers in Table A1 (10.6 W m$^{-2}$) and dividing this number by the standard deviation of the monthly STH–SLP index (1.68 mb) yielding $\alpha \simeq 6$ W m$^{-2}$ mb$^{-1}$. Figure 3c was computed with $w_* = 2$ m s$^{-1}$ and $C_E = 2/3 C_E^{\text{ref}}$, where $C_E^{\text{ref}} = 1.5 \times 10^{-3}$ is a reference value given in Gill (1982).

## REFERENCES

Carton, J. A., X. Cao, B. S. Giese, and A. M. da Silva, 1996: Deacadal and interannual SST variability in the tropical Atlantic. *J. Phys. Oceanogr.*, **26,** 1165–1175.

Chang, P., L. Ji, and H. Li, 1997: A decadal climate variation in the tropical Atlantic Ocean from thermodynamic air–sea interactions. *Nature*, **385,** 516–518.

——, R. Saravanan, L. Ji, and G. C. Hegerl, 2000: The effect of local sea surface temperature on atmospheric circulation over the tropical Atlantic sector. *J. Climate*, **13,** 2195–2216.

——, L. Ji, and R. Saravanan, 2001: A hybrid coupled model study of the tropical Atlantic variability. *J. Climate*, **14,** 361–390.

Chiang, J. C. H., S. Zebiak, and M. A. Cane, 2001: Related roles of elevated heating and surface temperature gradients in driving anomalous surface winds over tropical oceans. *J. Atmos. Sci.*, **58,** 1371–1394.

——, Y. Kushnir, and A. Giannini, 2002: Deconstructing Atlantic ITCZ variability: Influence of the local cross-equatorial SST

gradient, and remote forcing from the eastern equatorial Pacific. *J. Geophys. Res.,* **107** (D1), 1–19.
Covey, D., and S. Hastenrath, 1978: The Pacific El Niño phenomenon and the Atlantic circulation. *Mon. Wea. Rev.,* **106,** 1280–1287.
Curtis, S., and S. Hastenrath, 1995: Forcing of anomalous sea surface temperature evolution in the tropical Atlantic during Pacific warm events. *J. Geophys. Res.,* **100** (C8), 15 835–15 847.
Czaja, A., and J. Marshall, 2001: Observations of atmosphere–ocean coupling in the North Atlantic. *Quart. J. Roy. Meteor. Soc.,* **127,** 1893–1916.
Dommenget, D., and M. Latif, 2000: Interannual to decadal variability in the tropical Atlantic. *J. Climate,* **13,** 777–792.
Eden, C., and T. Jung, 2001: North Atlantic interdecadal variability: Oceanic response to the North Atlantic Oscillation (1865–1997). *J. Climate,* **14,** 676–691.
Enfield, D. B., and D. A. Mayer, 1997: Tropical Atlantic sea surface temperature variability and its relation to El Niño–Southern Oscillation. *J. Geophys. Res.,* **102,** 929–945.
Frankignoul, C., 1985: Sea surface temperature anomalies, planetary waves and air–sea feedbacks in the middle latitude. *Rev. Geophys.,* **23,** 357–390.
——, and K. Hasselman, 1977: Stochastic climate models. Part II: Application to sea-surface temperature variability and thermocline variability. *Tellus,* **29,** 289–305.
——, A. Czaja, and B. L'Hévéder, 1998: Air–sea feedback in the North Atlantic and surface boundary conditions for ocean models. *J. Climate,* **11,** 2310–2324.
Giannini, A., M. A. Cane, and Y. Kushnir, 2001: Interdecadal changes in the ENSO teleconnection to the Caribbean region and the North Atlantic Oscillation. *J. Climate,* **14,** 2867–2879.
Gill, A. E., 1982: *Atmosphere–Ocean Dynamics.* International Geophysical Series, Vol. 30, Academic Press, 662 pp.
Grötzner, A., M. Latif, and T. P. Barnett, 1998: A decadal climate cycle in the North Atlantic Ocean as simulated by the ECHO coupled GCM. *J. Climate,* **11,** 831–847.
Häkkinen, S., 1999: Variability of the simulated meridional heat transport in the North Atlantic for the period 1951–1993. *J. Geophys. Res.,* **104** (C5), 10 991–11 007.
Halliwell, G. R., 1998: Simulation of North Atlantic decadal/multidecadal winter SST anomalies driven by basin-scale atmospheric circulation anomalies. *J. Phys. Oceanogr.,* **28,** 5–21.
——, and D. A. Mayer, 1996: Frequency response properties of forced climatic SST anomaly variability in the North Atlantic. *J. Climate,* **9,** 3575–3587.
Hastenrath, S., and L. Greischar, 1993: Circulation mechanisms related to Northeast Brazil rainfall anomalies. *J. Geophys. Res.,* **98** (D3), 5093–5102.
Hurrell, J., 1995: Decadal trends in the North Atlantic Oscillation: Regional temperature and precipitation. *Science,* **269,** 676–679.
Kalnay, E., and Coauthors, 1996: The NCEP/NCAR 40-Year Reanalysis Project. *Bull. Amer. Meteor. Soc.,* **77,** 437–471.
Kaplan, A., Y. Kushnir, M. Cane, and B. Blumenthal, 1997: Reduced space optimal analysis for historical datasets: 136 years of Atlantic sea surface temperatures. *J. Geophys. Res.,* **102,** 27 835–27 860.
——, ——, and ——, 2000: Reduced space optimal interpolation of historical marine sea level pressure: 1854–1992. *J. Climate,* **13,** 2987–3002.
Klein, S. A., B. J. Soden, and N.-C. Lau, 1999: Remote sea surface variations during ENSO: Evidence for a tropical atmospheric bridge. *J. Climate,* **12,** 917–932.
Levitus, S., and T. Boyer, 1994: *Temperature.* Vol 4, *World Ocean Atlas 1994,* NOAA Atlas NESDIS 4, 117 pp.
Marshall, J., and Coauthors, 2001: Atlantic climate variability. *Int. J. Climatol.,* **21,** 1863–1898.
Nobre, P., and J. Shukla, 1996: Variations in sea surface temperature, wind stress, and rainfall over the tropical Atlantic and South America. *J. Climate,* **9,** 2464–2479.
Percival, D. B., and T. A. Walden, 1993: *Spectral Analysis for Physical Applications: Multitaper and Conventionnal Univariate Techniques.* Cambridge University Press, 583 pp.
Philander, S. G. H., 1990: *El Niño, La Niña, and the Southern Oscillation.* International Geophysics Series, Vol. 46, Academic Press, 293 pp.
Saravanan, R., and P. Chang, 2000: Interaction between tropical Atlantic variability and El Niño–Southern Oscillation. *J. Climate,* **13,** 2177–2194.
Seager, R., Y. Kushnir, P. Chang, N. Naik, J. Miller, and W. Hazeleger, 2001: Looking for the role of ocean in tropical Atlantic decadal climate variability. *J. Climate,* **14,** 638–655.
Sutton, R. T., S. P. Jewson, and D. P. Rowell, 2000: The elements of climate variability in the tropical Atlantic region. *J. Climate,* **13,** 3261–3284.
Trenberth, K. E., 1984: Signal versus noise in the Southern Oscillation. *Mon. Wea. Rev.,* **112,** 326–332.
——, D. P. Stepaniak, and J. W. Hurrell, 2001: Quality of reanalyses in the Tropics. *J. Climate,* **14,** 1499–1510.
Wunsch, C., 1999: The interpretation of short climate records, with comments on the North Atlantic Oscillation and Southern Oscillations. *Bull. Amer. Meteor. Soc.,* **80,** 245–255.
Xie, S. P., 1999: A dynamic ocean–atmosphere model of the tropical Atlantic decadal variability. *J. Climate,* **12,** 64–70.
——, and S. G. H. Philander, 1994: A coupled ocean–atmosphere model of relevance to the ITCZ in the eastern Pacific. *Tellus,* **46A,** 340–350.